ACS APPLIED ENERGY MATERIALS

www.acsaem.org Article

Improved Single-Ion Conductivity of Polymer Electrolyte via Accelerated Segmental Dynamics

Sheng Zhao, Yiman Zhang, Hoang Pham, Jan-Michael Y. Carrillo, Bobby G. Sumpter, Jagjit Nanda, Nancy J. Dudney, Tomonori Saito, Alexei P. Sokolov,* and Peng-Fei Cao*

Cite This: *ACS Appl. Energy Mater.* 2020, 3, 12540−12548 Read Online

ACCESS | Metrics & More | Article Recommendations | Supporting Information

ABSTRACT: Single-ion conducting polymer electrolytes (SICPEs) have many advantages for solid-state battery applications, while low conductivities remain the bottleneck for their practical applications. Herein, a strategy that can significantly improve the ionic conductivity of SICPEs based on the concept of accelerated segmental dynamics was demonstrated by the evaluation of the thermal property, rheological behavior, morphology analysis, molecular dynamics simulation, and conductivity performance. With both "soft" poly(dimethylsiloxane) (PDMS) backbone and poly(ethylene glycol) (PEG) side chains, the obtained SICPE possesses faster segmental relaxation and higher lithium-ion conductivity. With lithium "transference" number close to unity, the obtained SICPE also shows excellent electrochemical stability against lithium metal electrodes. The clear relationship established between the segmental dynamics of polymer electrolyte and its ionic conductivity should contribute to achieve a solid electrolyte with improved ionic conductivity toward the next-generation solid-state battery.

KEYWORDS: *single ion conducting, polymer electrolyte, "soft" structure, poly(dimethylsiloxane), segmental dynamics*

■ INTRODUCTION

Solid-state batteries (SSB) are considered as the holy grail of next-generation battery technology with higher energy density and enhanced safety. To achieve this technological breakthrough, solid electrolytes need to have ionic conductivity close to that of current liquid electrolytes with good interfacial stability.[1−7] With their inherent design flexibility, nonflammable, scalable membrane formation, and tunable mechanical property, polymer electrolytes have emerged as one of the most promising candidates for SSB.[8−23] However, the traditional lithium-salt-doped poly(ethylene oxide) (PEO) usually suffers from low lithium-ion "transference" number (t_{Li}^{+} < 0.4) that renders numerous problems, such as electrode polarization, ion concentration gradient, and undesirable side reactions.[10] By covalently attaching anions to the polymer backbone, single-ion conducting polymer electrolytes (SICPEs) have been fabricated to resolve these problems.[11,24−33] Simulation results showed that even with slightly lower conductivity, SICPEs still provide higher power density and enable faster charging in comparison to traditional liquid electrolytes.[34] Recent reports also demonstrated that single-ion conductors suppress the dendrite growth on Li metal electrodes, enabling stable and safe Li metal-based batteries.[24,26,27,35−41] However, the low ionic conductivity of SICPEs in comparison to traditional liquid electrolyte remains a bottleneck for their practical applications.[11]

Fabrication of weakly coordinating anions with a highly delocalized negative charge is especially useful in improving the ionic conductivity of SICPEs, and the approach mainly relies on polymers with ionic-liquid-like monomers, backbone, or side chains.[25,42−44] Polyanions with sulfonyl-(trifluoromethanesulfonyl)imide structure (SO_2-$N^{(-)}$-SO_2-CF_3) are usually employed to synthesize SICPEs with high ionic conductivity.[11,36,45] Further improvement was also reported by replacing one ═O group in the above structure by a stronger electron-withdrawing group rendering a super-delocalized polyanion.[44] However, these homopolymers, including lithium poly(4-styrenesulfonyl)-(trifluoromethanesulfonyl)imide (LiPSTFSI),[30,46] lithium poly 1-[3-(methacryloyloxy)propylsulonyl]-1-(trifluoromethanesulfonyl)imide (LiPMTFSI),[47] and lithium

Received: October 8, 2020
Accepted: November 13, 2020
Published: December 7, 2020

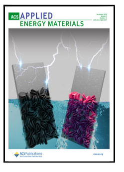

https://dx.doi.org/10.1021/acsaem.0c02079
ACS Appl. Energy Mater. 2020, 3, 12540−12548

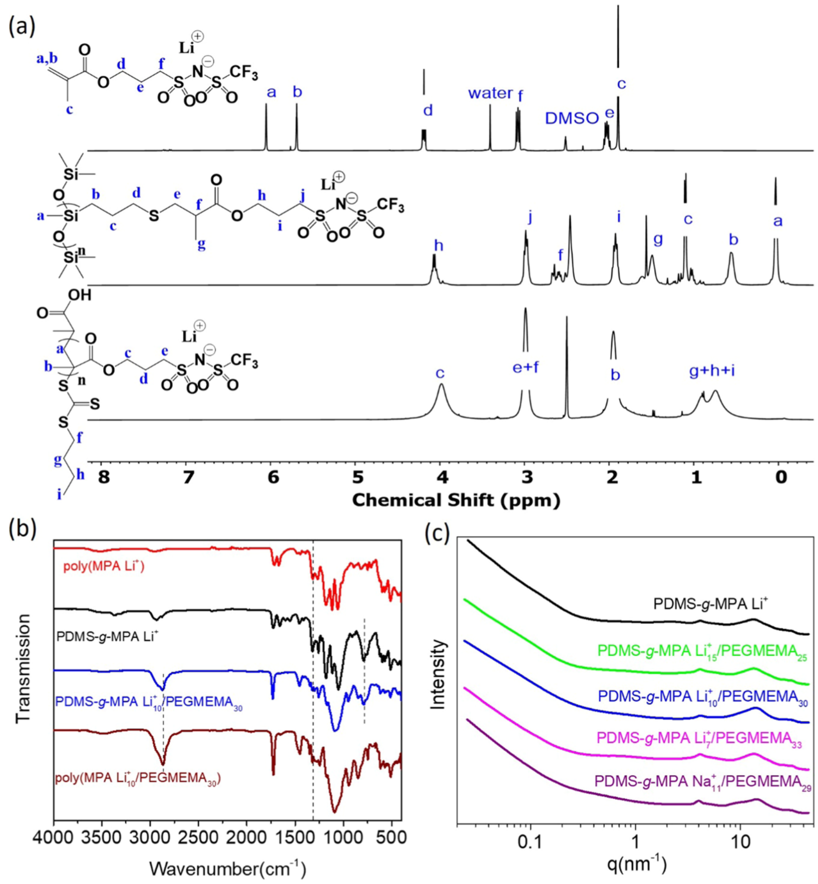

Figure 1. (a) ^{1}H NMR spectra of MPA Li$^+$ monomer, PDMS-*g*-MPA Li$^+$, and poly(MPA Li$^+$) in DMSO. (b) FT-IR spectra of poly(MPA Li$^+$), PDMS-*g*-MPA Li$^+$, PDMS-*g*-MPA Li^+_{10}/$PEGMEMA_{30}$, and poly(MPA Li^+_{10}/$PEGMEMA_{30}$). (c) SAXS−WAXS profiles of PDMS-*g*-MPA Li$^+$, PDMS-*g*-MPA Li^+_x/$PEGMEMA_y$, and PDMS-g-MPA Na^+_{10}/$PEGMEMA_{30}$.

poly[(4-styrenesulfonyl)(trifluoromethyl(S-trifluoromethylsulfonylimino) sulfonyl)imide] (LiPSsTFSI),[48] have high glass transition temperature (T_g) and always suffer from very low ionic conductivity at ambient temperature. Accelerating the segmental dynamics by incorporation of low-T_g polymer segments is an efficient way to improve the ionic conductivity of SICPEs.[25,30,48] Aside from physical blending, the current research is mainly focusing on covalently grafting a SICPE block to one or both sides of high-molecular-weight (M_W) PEO, or on copolymerization with the low M_W PEO ($T_g \sim -60$ °C).[25,49,50] Matyjaszewski and co-workers also reported homopolymer SICPEs with a PEO spacer between the single-ion conducting units and the polymer backbone.[51] There have been numerous attempts on modifying the side chain, but only a few attempts have been made on tuning the polymer backbones of sulfonyl(trifluoromethanesulfonyl)imide-based SICPEs,[11,52,53] which may significantly influence segmental dynamics.[30]

Herein, we introduce a novel SICPE with both a "soft" polymer backbone and side chain that provides accelerated segmental dynamics. Compared to traditional "rigid" polymer backbones, such as poly(methyl methacrylate) (PMMA), the soft poly(dimethylsiloxane) (PDMS) ($T_g \sim -120$ °C) backbone exhibits much faster segmental dynamics (shorter relaxation time) and hence higher conductivity (6 orders of magnitude improvement). Further cografting with PEO side chains results in the SICPEs with further accelerated segmental dynamics that provides significantly improved conductivity in comparison to the state-of-the-art sulfonyl(trifluoromethanesulfonyl)imide-based SICPE.

RESULTS AND DISCUSSION

The detailed synthesis procedures are included in the Supporting Information. The lithium 1-[3-(methacryloyloxy)propylsulfonyl]-1-(trifluoromethanesulfonyl)-imide (MPA Li$^+$) monomer was synthesized with chemical structure verified by ^{1}H nuclear magnetic resonance (^{1}H NMR) and ^{19}F NMR spectrum (Figures 1a and S1). The PDMS-based SICPEs, i.e., PDMS-*g*-MPA Li$^+$ or PDMS-*g*-MPA Li^+_x/$PEGMEMA_y$, were synthesized by chemical grafting of MPA Li$^+$ or cografting with a varied molar ratio of poly(ethylene glycol) methyl ether methacrylate (PEGMEMA) on (mercaptopropyl)-methylsiloxane (PDMS-SH) via a thiol-ene reaction (Scheme 1a top). Poly(MPA Li$^+$) was synthesized as the control to evaluate the influence of accelerated segmental dynamics on the single-ion conductivity of PDMS-based SICPEs. Poly(MPA Li$^+$) and poly(MPA Li^+_x/$PEGMEMA_y$) were synthesized by reversible addition fragmentation chain-transfer (RAFT) polymerization of the same monomers (Scheme 1a bottom). The molar ratio of monomers to RAFT-CTA was chosen specifically to have a comparable number of functional units per molecule, i.e., degree of polymerization (DP_n), with PDMS-based SICPEs. Their chemical structures were verified by ^{1}H NMR and Fourier transform infrared (FT-IR) spectroscopy. The absence of proton signals between 5.5 and 6.6 ppm corresponding to the alkene group in the ^{1}H NMR spectra of all SICPEs

Scheme 1. (a) Synthesis of a PDMS Backboned SICPEs via Thiol-Ene Reaction and Methyl Methacrylate Backbones SICPEs via Reversible Addition Fragmentation Chain-Transfer (RAFT) Polymerization. (Note: PDMS-g-MPA Li$^+$/PEGMEMA Refers to Both MPA Li$^+$ and PEGMEMA, Which Were Chemically Grafted on PDMS Backbone.) (b) Included Cartoons of SICPEs Demonstrate the Relative Flexibility of Their Backbone and Side Chain. (c) Snapshots of Simulation Cells Containing a Coarse-Grained Model Representing Flexible-Backbone PDMS-g-MPA Li$^+_{10}$/PEGMEMA$_{30}$ and Rigid-Backbone Poly(MPA Li$^+_{10}$/PEGMEMA$_{30}$)[a]

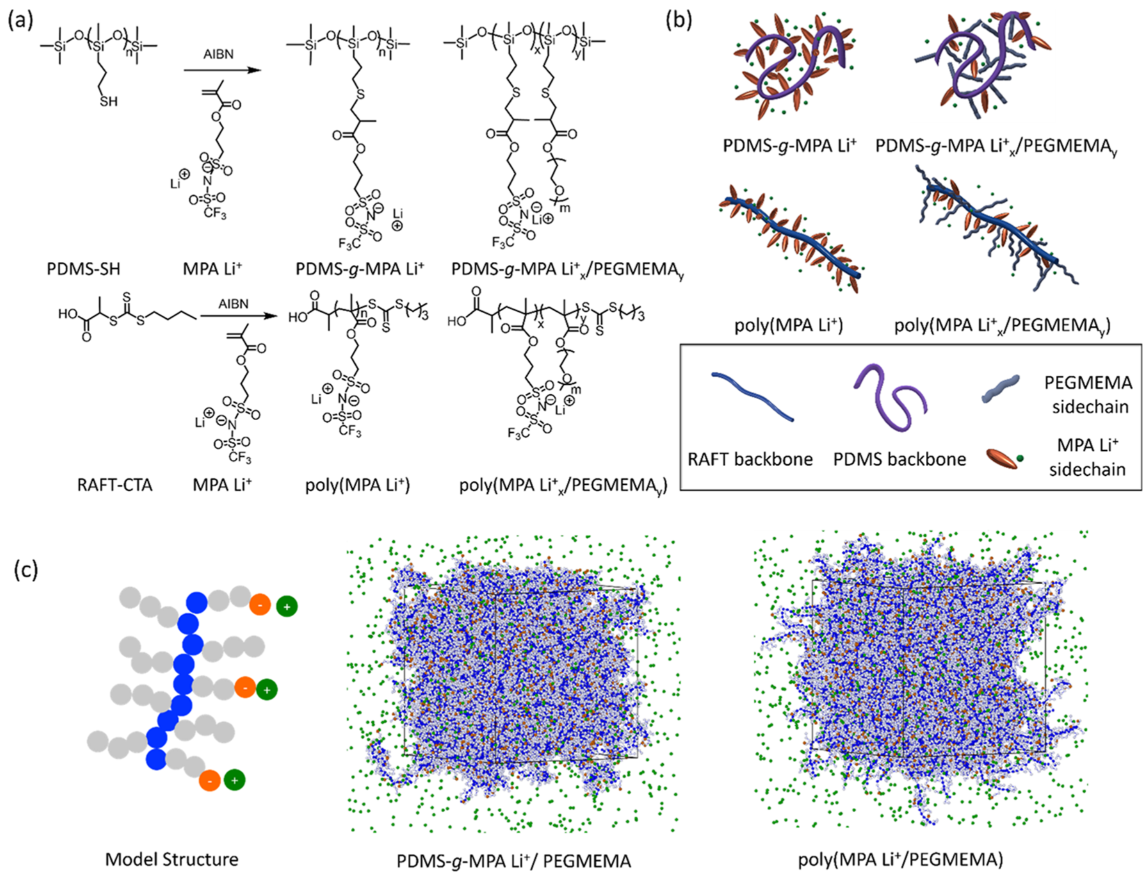

[a]The color-coding scheme is used to show the main chain (blue beads), grafted side chains (silver beads for neutral grafted chains and orange beads for negatively charged chain ends), and lithium ions (green beads).

Table 1. Summary of Thermal Property and Conductivity of SICPE

	T_g (°C)				
	DSC	rheometer	BDS	$T_{d,5\%}$ (°C)[a]	σ at 30 °C (S/cm)
poly(MPA Li$^+$)	152.8		150.1	226.9	<10^{-15}
PDMS-g-MPA Li$^+$	31.8	34.8	30.6	271.0	5.9×10^{-15}
PDMS-g-MPA Li$^+_{15}$/PEGMEMA$_{25}$	−46.7	−48.5	−51.2	331.7	2.6×10^{-6}
PDMS-g-MPA Li$^+_{10}$/PEGMEMA$_{30}$	−55.2	−57.8	−59.2	325.1	4.2×10^{-6}
PDMS-g-MPA Li$^+_{7}$/PEGMEMA$_{33}$	−60.2	−64.4	−62.8	340.3	2.7×10^{-6}
poly(MPA Li$^+_{10}$/PEGMEMA$_{30}$)	−45.5	−44.5	−49.6	326.3	4.6×10^{-7}
PDMS-g-MPA Na$^+_{11}$/PEGMEMA$_{29}$	−51.4	−53.4	−52.2	335.4	9.1×10^{-7}
poly(MPA Na$^+_{11}$/PEGMEMA$_{29}$)	−37.7	−34.8	−38.7	328.2	1.61×10^{-7}

[a]This parameter implies the temperature when the weight loss of samples is 5%.

demonstrated the complete removal of free monomers from the obtained polymers (Figures 1a, S2, and S3). As illustrated by the IR spectra of PDMS-g-MPA Li$^+$ and PDMS-g-MPA Li^+_x/PEGMEMA$_y$, the strong peak at 796 cm^{-1} corresponding to the deformation mode of Si−O−Si,[54] and the absence of a peak at 2550 cm^{-1} corresponding to the stretching mode of S−H bond suggested the complete conversion of thiol units (Figures 1b and S4). This point could also be proven by the equal integrals of the peaks at 0.5−0.7 ppm (−CH$_2$− connected to silicon) and 4.1−4.3 ppm (−CH$_2$− adjacent to ester units) in the ^{1}H NMR spectrum. For PDMS-g-MPA Li^+_x/PEGMEMA$_y$ and poly(MPA Li^+_x/PEGMEMA$_y$), with fixed peak intensity at 1320 cm^{-1} (S═O rocking mode), the relatively higher intensity of the peak at 2880 cm^{-1} (C−H stretching mode from PEGMEMA) demonstrated the increased PEGMEMA content in the polymers following the increased feed ratio of PEGMEMA to MPA Li$^+$ (Figure S4b). In their ^{1}H NMR spectra, both MPA Li$^+$ and PEGMEMA have

https://dx.doi.org/10.1021/acsaem.0c02079
ACS Appl. Energy Mater. 2020, 3, 12540−12548

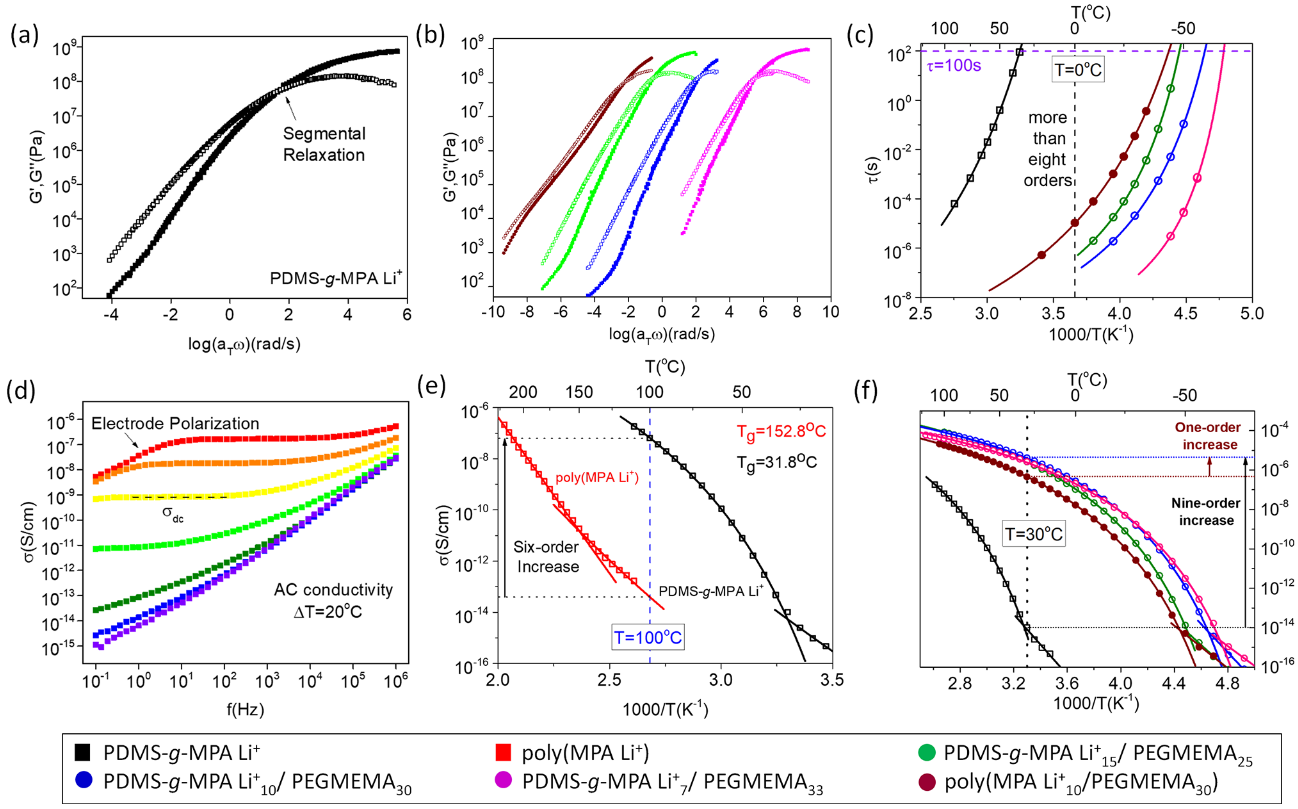

Figure 2. Master curves of storage modulus G' (solid) and loss modulus G'' (empty) for (a) PDMS-*g*-MPA Li^+ at 60 °C and (b) PDMS-*g*-MPA Li^+_x/PEGMEMA$_y$ and poly(MPA Li^+_{10}/PEGMEMA$_{30}$) at −45 °C. (c) Estimation of their segmental relaxation times vs 1000/T. (d) Real part of conductivity (σ') for PDMS-*g*-MPA Li^+ from 110 to −10 °C. Conductivity vs 1000/T of (e) PDMS-*g*-MPA Li^+ and poly(MPA Li^+), (f) PDMS-*g*-MPA Li^+, PDMS-*g*-MPA Li^+_x/PEGMEMA$_y$, and poly(MPA Li^+_{10}/PEGMEMA$_{30}$). The data points of segmental relaxation time and conductivity were fitted by the VFT equation above T_g and the Arrhenius equation below T_g (solid lines). The segmental relaxation time and conductivity at the chosen temperature (0 °C in (c), 100 °C in (e), and 30 °C in (f)) are marked with a dashed line. The list of symbols: PDMS-*g*-MPA Li^+ (black box), poly(MPA Li^+) (red box), PDMS-*g*-MPA Li^+_{15}/PEGMEMA$_{25}$ (green circle open), PDMS-*g*-MPA Li^+_{10}/PEGMEMA$_{30}$ (blue circle open), PDMS-*g*-MPA Li^+_7/PEGMEMA$_{33}$ (pink circle open), and poly(MPA Li^+_{10}/PEGMEMA$_{30}$) (wine circle solid).

a common peak between 4.1 and 4.3 ppm corresponding to the $-CH_2-$ adjacent to ester units, whereas the $-CH_2CH_2-$ units connected with $-SO_2-$ in the MPA Li^+ show two separate peaks between 2.1−2.3 and 3.1−3.3 ppm. The calculated mole ratios of PEGMEMA over MPA Li^+ based on the integration values of these peaks are slightly higher than their feed ratios, which may be explained by the relatively higher reactivity of PEGMEMA than MPA Li^+ during the polymerization process.

Poly(MPA Li^+) possesses a high T_g value of 152 °C and hence a very low Li^+ conductivity, which is out of the measurement range at 30 °C (<10^{-15} S/cm) and is only 3.9 × 10^{-14} S/cm at 100 °C (Table 1). The first acceleration of segmental dynamics is achieved by changing the rigid PMMA backbone to a soft PDMS backbone. First, the PDMS-*g*-MPA Li^+ shows a much better thermal stability in comparison to that obtained for poly(MPA Li^+) perhaps due to the absence of a trithiocarbonate bond in RAFT-CTA (Figure S5a).[12,55,56] With the hydrophilic MPA Li^+ grafted on a hydrophobic PDMS backbone, there are no defined peaks observed in the small-angle X-ray scattering (SAXS) and wide-angle X-ray scattering (WAXS) spectra of PDMS-*g*-MPA Li^+ (Figure 1c). Combined with the presence of only one T_g in the measured temperature range of differential scanning calorimetry (DSC), it suggests the absence of microphase separation between PDMS backbone and grafted side chains (Figure S6a). The absence of phase separation is important for efficient acceleration of the segmental dynamics via a soft backbone effect. The segmental relaxation time for PDMS-*g*-MPA Li^+ at different temperatures was estimated from a master curve by rheological measurement and plotted in Figure 2c, whose detailed procedure is included in the Supporting Information. Unfortunately, no reliable rheological results were obtained for poly(MPA Li^+) due to its rigid structure, which makes it impossible to directly compare the segmental relaxation time between FPDMS-*g*-MPA Li^+ and poly(MPA Li^+). However, the significant drop in T_g (~120 °C) suggests faster segmental dynamics at the same temperature (Figure S6a). The conductivity of SICPEs was measured by broadband dielectric spectroscopy (BDS) over a broad temperature range. As all studied SICPEs show similar responses in the real part of the conductivity (σ') spectrum, the σ' spectrum of PDMS-*g*-MPA Li^+ is included as an example in Figure 2d and the detailed analysis procedure is included in the Supporting Information. For SICPEs, the conductivity is determined by both concentration and mobility of the free ions. Since lithium ions have relatively weak electrostatic interaction with the bulky TFSI anion, partially dissociated lithium ions could still transform through ion hopping even when the side chain is frozen. Therefore, the ionic conductivity is decoupling from the segmental relaxation for poly(MPA Li^+). With no phase separation observed between the polymer backbone and side chains for PDMS-*g*-MPA Li^+, the flexible PDMS backbone

https://dx.doi.org/10.1021/acsaem.0c02079
ACS Appl. Energy Mater. 2020, 3, 12540−12548

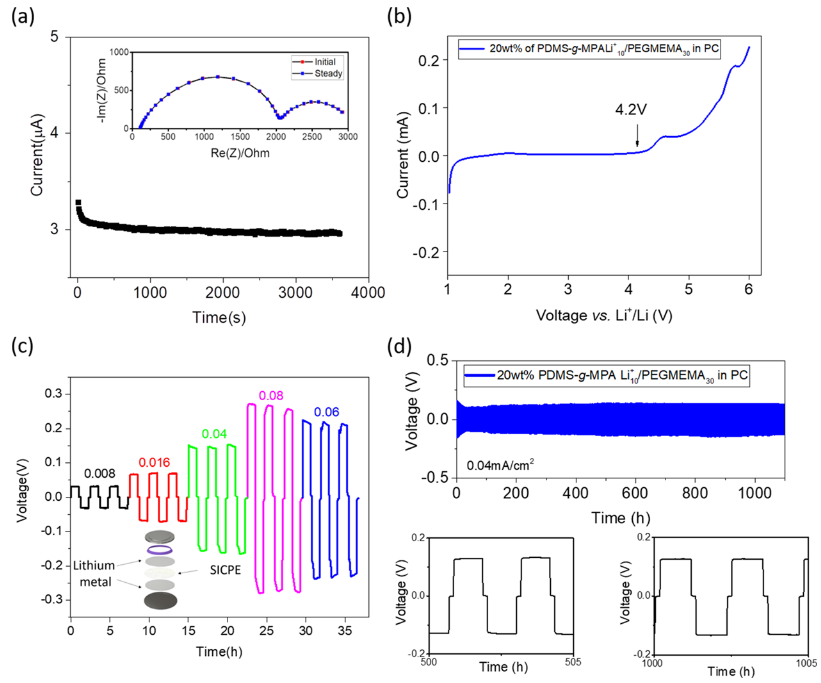

Figure 3. Electrochemical performance of PC-doped PDMS-*g*-MPA Li^+_{10}/$PEGMEMA_{30}$. (a) Chronoamperometry (CA) response of the Li/Li symmetric cell under 10 mV polarization voltage and electrochemical impedance spectroscopy (EIS) spectra before and after dc polarization (inset). (b) Electrochemical stability of the Li/SS cell using the linear sweep voltammetry (LSV) from 1.0 to 6.0 V vs Li/Li^+ with a sweep rate of 5 mV/s. (c) Voltage profile of the Li/Li symmetric cell subjected to elevated currents of 0.008, 0.016, 0.04, and 0.8 mA/cm^2 (electrode diameter = 1.27 cm, surface area = 1.27 cm^2), followed by lowering the current to 0.06 mA/cm^2, for a series of lithium plating/tripping cycles. (d) Long-term galvanostatic cycling test of the Li/Li symmetric cell at a constant current of 0.04 mA/cm^2 up to 1100 h, and selected cycles around 500 and 1000 h.

would cause relatively dense packing of MPA Li^+ side chains and accelerate the transport of lithium ions efficiently. As the dynamics of lithium ions are strongly coupled with segmental dynamics for PDMS-*g*-MPA Li^+ in our system,[57] the ionic conductivity of PDMS-*g*-MPA Li^+ is more than 6 orders of magnitude higher than that of in poly(MPA Li^+) (3.9×10^{-14} S/cm vs 6.9×10^{-8} S/cm at 100 °C) (Figure 2e).

Though the single-ion conductivity was improved by 6 orders of magnitude after replacing the PMMA backbone with PDMS one, the ionic conductivity of PDMS-*g*-MPA Li^+ at ambient temperature is far below that required for practical applications in batteries. Therefore, in addition to the soft backbone, we also performed side chain modification via cografting the PEGMEMA monomer. With flexible PEGMEMA side chains cografted on the PDMS backbone, PDMS-*g*-MPA Li^+_{15}/$PEGMEMA_{25}$ exhibits significantly accelerated segmental dynamics with relaxation time shorter than 10^{-6} s at 0°C, which is more than 8 orders of magnitude faster than that of PDMS-*g*-MPA Li^+ at the same temperature (>100 s, Figure 2c). The segmental dynamics can be further accelerated with an increasing molar ratio of PEGMEMA to MPA Li^+. The accelerated segmental dynamics was also confirmed by the significantly reduced T_g value (Figure S6b). With an equal feed ratio of PEGMEMA to MPA Li^+ grafted on PDMS backbone, the T_g of PDMS-*g*-MPA Li^+_{15}/$PEGMEMA_{25}$ decreased to −45°C. Increasing the feed ratio of PEGMEMA and MPA Li^+ to two and three, the T_g of PDMS-*g*-MPA Li^+_{10}/$PEGMEMA_{30}$ and PDMS-*g*-MPA Li^+_7/$PEGMEMA_{33}$ further decreased to −55 and −60 °C, with the latter value being close to the T_g of PEO. The high ratio of PEGMEMA inside the PDMS-*g*-MPA Li^+_7/$PEGMEMA_{33}$ even results in a crystalline structure observed only in the heating cycle of the DSC curves. The crystallization was also observed in the rheology measurement, where it caused failure of time-temperature-superposition (TTS) in the construction of master curve at −40°C (Figure 2b).

Comparing with PDMS-*g*-MPA Li^+, the ionic conductivity of PDMS-*g*-MPA Li^+_x/$PEGMEMA_y$ is increased by 9 orders of magnitude due to the accelerated segmental dynamic via cografting with PEGMEMA monomers (∼10^{-6} S/cm vs 6×10^{-15} S/cm at 30 °C in Figure 2f). It is noteworthy that although the segmental relaxation time of PDMS-*g*-MPA Li^x_+/$PEGMEMA_y$ decreases significantly with the increasing ratio of PEGMEMA, the ionic conductivity is not always improved. This is because the increased ratio of PEGMEMA will not only accelerate segmental dynamics but also decrease the Li^+ concentration at the same time. Therefore, the conductivity would reach a maximum value only when the ratio between PEGMEMA and MPA Li^+, i.e., the ratio of ethylene oxide group (EO) to Li^+, reaches an optimal value. The relationship between conductivity and ratio of EO/Li^+ has been widely studied for lithium-salt-doped PEO, and the optimal ratio may be varied from 9 to 24 depending on the types of lithium salt.[58,59] The highest conductivity ∼ 4.3×10^{-6} S/cm at 30 °C was reached in PDMS-*g*-MPA Li^+_{10}/$PEGMEMA_{30}$ with EO/Li^+ ratio ∼27:1. This single lithium-ion conductivity value is several orders of magnitude higher than those achieved in structures containing PEO in the backbone[25,50] and half-order higher than the reported sulfonyl(trifluoromethanesulfonyl)-imide-based SICPEs with PEO block as side chains (Table S1).[47,60]

With optimal EO/Li^+ ratio, the copolymer of MPA Li^+ and PEGMEMA has been reported as one of the state-of-the-art SICPEs with the highest lithium ionic conductivity.[47] Therefore, poly(MPA Li^+_{10}/$PEGMEMA_{30}$) was also synthesized as a control, which has the same ratio of EO/Li^+ and shows similar thermal stability (Figure S5b). So, the flexible PDMS backbone of PDMS-*g*-(MPA Li^+_{10}/$PEGMEMA_{30}$) would result in faster segmental dynamics than poly(MPA Li^+_{10}/$PEGMEMA_{30}$). As the PEO units would solvate lithium ions, the transportation of lithium ions is strongly coupled with the motion of PEO side chains. Therefore, the faster segmental dynamics of PDMS-*g*-(MPA Li^+_{10}/$PEGMEMA_{30}$) would allow faster lithium-ion transport for coupled systems. So PDMS-g-(MPA Li^+_{10}/$PEGMEMA_{30}$) has an order higher conductivity at room temperature. Compared with poly(MPA Li^+_{10}/$PEGMEMA_{30}$), the soft PDMS backbone makes the segmental dynamics of the PDMS-*g*-MPA Li^+_{10}/$PEGMEMA_{30}$ 2 orders of magnitude faster at the same temperature (10^{-7} s vs 10^{-5} s at 0 °C in Figure 2c). This faster segmental dynamics corresponds to a 9 °C decrease in T_g (−60.2 °C vs −51.4 °C in Figure S6b) and 1 order of magnitude higher lithium conductivity at 30 °C (4.7×10^{-6} S/cm vs 4.6×10^{-7} S/cm) than in poly(MPA Li^+_{10}/$PEGMEMA_{30}$) (Figure 2f). The accelerated segmental dynamics enabled by softening the backbone was also demonstrated by the mean square displacement (MSD) from coarse-grained molecular dynamics simulations (Scheme 1c). The computation results show that the dynamics of the backbones and side chains of the coarse-grained model with a soft backbone, representing PDMS-*g*-MPA Li^+_{10}/$PEGMEMA_{30}$ are significantly faster than the more rigid model representing poly(MPA Li^+_{10}/$PEGMEMA_{30}$) (Figure S15a,b). As lithium-ion diffusions are coupled with segmental dynamics for both SICPEs, the accelerated polymer dynamics results in a faster lithium-ion diffusion (Figure S15c), which emphasizes the importance of a soft backbone to accelerate segmental dynamics.

To further demonstrate the effect of accelerated segmental dynamics on the conductivity of other SICPEs, single sodium ion conducting polymer electrolytes have also been studied. The PDMS-based polymer electrolytes, i.e., PDMS-*g*-MPA Na^+_{11}/$PEGMEMA_{29}$, along with the control poly(MPA Na^+_{11}/$PEGMEMA_{29}$) were synthesized and verified with ^{1}H NMR spectra and FT-IR (Figures S7 and S8). Similarly with Li^+-conducting SICPEs, the soft PDMS backbone leads to a faster segmental dynamic in PDMS-*g*-(MPA Na^+_{11}/$PEGMEMA_{29}$) than that of in poly(MPA Na^+_{11}/$PEGMEMA_{29}$) (8×10^{-6} s vs 6×10^{-2} s at −20 °C in Figure S10b). This faster segmental dynamics also corresponds to a 13 °C lower T_g (−51 °C vs −38 °C in Figure S9b) and 1 order of magnitude higher sodium ion conductivity (10^{-6} S/cm vs 10^{-7} S/cm at 30 °C in Figure S11). This demonstrates the potential of accelerated segmental dynamics to improve the ionic conductivity of polymer electrolytes with different counter ions, like zinc,[61−63] magnesium,[64] and aluminum,[65] or charged units, like (fluorosulfonyl)imide.[33]

The transference number (strictly speaking, transport number t^+_{Li}) was measured via the potentio-static polarization method using a Li/Li symmetric cell.[66] With propylene carbonate (PC) as a plasticizer, the T_g of PDMS-*g*-MPA Li^+_{10}/$PEGMEMA_{30}$ was further decreased to −113 °C (Figure S12a) and conductivity at room temperature was improved by 1.5 orders of magnitude (~1.0×10^{-4} S/cm at 30 °C in Figure S12b). The obtained t^+_{Li} was determined to be 0.85 (Figure 3a), which is comparable with other reported single-ion conducting polymer electrolyte systems,[26,50,52,67−73] and much higher than a normal dual-ion polymer electrolyte systems with values of around 0.37 (Table S1).[74−80] The electrochemical stability of the obtained SICPE was tested by linear sweep voltammetry (LSV) using Li/stainless steel cell, as shown in Figures 3b and S13. There is no obvious anodic current peak till 4 V for both dry and PC-doped PDMS-*g*-MPA Li^+_{10}/$PEGMEMA_{30}$, indicating their excellent electrochemical stability. To further evaluate the stability of the obtained SICPE against lithium metal electrodes, the Li/Li symmetric cell with the same PC-doped PDMS-*g*-MPA Li^+_{10}/$PEGMEMA_{30}$ electrolyte was assembled and tested by performing galvanostatic stripping/plating processes under various current densities. As illustrated in Figure 3c, the voltage profile shows a stable response under varied current densities. In addition, the long-term endurance test for more than 1100 h was also performed (Figure 3d). The overpotential is slightly decreasing at initial cycles, followed by a gradual increase and eventually stabilizing after 30 h. This slight variation at initial cycles is related to the reorganizing process on the lithium metal surface before the final steady state.[27] No short circuit or other significant change was observed in the long-term voltage profile. In addition, the cells after the galvanostatic cycling test were disassembled in an argon-protected glovebox, and no significant corrosion was observed on the lithium metal electrode (Figure S14), thus demonstrating a relatively stable solid electrolyte interface (SEI) layer between the SICPE and lithium metal electrode (Figure 3d).[81]

■ CONCLUSIONS

In this article, we demonstrated a strategy to significantly improve the Li ionic conductivity of SICPEs based on the concept of accelerated segmental dynamics in polymer design. A series of SICPEs with both soft PDMS polymer backbone and PEGMEMA side chains were synthesized by a one-pot thiol-ene reaction. In comparison to the SICPE with a rigid PMMA backbone, the SICPE with accelerated segmental dynamics, i.e., PDMS-*g*-MPA Li^+_x/$PEGMEMA_y$, showed a much faster segmental dynamics and several orders of magnitude higher single-ion conductivity, with PDMS-*g*-MPA Li^+_{10}/$PEGMEMA_{30}$ achieving the lithium conductivity of 4.7×10^{-6} S/cm at ambient temperature. Molecular dynamics simulations conducted with the flexible-backbone PDMS-*g*-MPA Li^+_{10}/$PEGMEMA_{30}$ and the rigid-backbone poly(MPA Li^+_{10}/$PEGMEMA_{30}$) showed faster dynamics for all parts of PDMS-*g*-MPA Li^+_{10}/$PEGMEMA_{30}$, i.e., main chain, side chains, and lithium ions, emphasizing the importance of accelerated segmental dynamics enabled by softening the backbone. We also demonstrate that the developed concept is able to improve the conductivity of other SICPEs, e.g., single sodium ion conducting polymer electrolyte. With transference number around 0.85, the assembled Li/Li symmetric cell with PC-doped SICPE, i.e., PDMS-*g*-MPA Li^+_{10}/$PEGMEMA_{30}$, also shows excellent electrochemical stability against lithium metal electrodes. The present study demonstrates the clear relationship between the segmental dynamic of SICPEs with their ionic conductivity, and the concept of accelerated segmental dynamics can also be applied to other types of polymer electrolytes, contributing to achieve high-performance solid-state electrolyte.

■ ASSOCIATED CONTENT

Supporting Information

The Supporting Information is available free of charge at https://pubs.acs.org/doi/10.1021/acsaem.0c02079.

https://dx.doi.org/10.1021/acsaem.0c02079
ACS Appl. Energy Mater. 2020, 3, 12540−12548

Synthesis of SICPEs; TGA traces and DSC curves for SICPEs; evaluation of properties for SICPEs with Na^+; mean square displacement (MSD) simulations for PDMS-g-MPA Li^+_{10}/$PEGMEMA_{30}$ and poly(MPA Li^+_{10}/$PEGMEMA_{30}$) (PDF)

AUTHOR INFORMATION

Corresponding Authors

Alexei P. Sokolov − *Chemical Sciences Division, Oak Ridge National Laboratory, Oak Ridge, Tennessee 37830, United States; Department of Chemistry, University of Tennessee, Knoxville, Tennessee 37996, United States;* orcid.org/0000-0002-8187-9445; Email: sokolov@utk.edu

Peng-Fei Cao − *Chemical Sciences Division, Oak Ridge National Laboratory, Oak Ridge, Tennessee 37830, United States;* orcid.org/0000-0003-2391-1838; Email: caop@ornl.gov

Authors

Sheng Zhao − *Department of Chemistry, University of Tennessee, Knoxville, Tennessee 37996, United States*

Yiman Zhang − *Chemical Sciences Division, Oak Ridge National Laboratory, Oak Ridge, Tennessee 37830, United States;* orcid.org/0000-0002-5468-7181

Hoang Pham − *Chemical Sciences Division, Oak Ridge National Laboratory, Oak Ridge, Tennessee 37830, United States*

Jan-Michael Y. Carrillo − *Center for Nanophase Materials Sciences, Oak Ridge National Laboratory, Oak Ridge, Tennessee 37830, United States;* orcid.org/0000-0001-8774-697X

Bobby G. Sumpter − *Center for Nanophase Materials Sciences, Oak Ridge National Laboratory, Oak Ridge, Tennessee 37830, United States;* orcid.org/0000-0001-6341-0355

Jagjit Nanda − *Chemical Sciences Division, Oak Ridge National Laboratory, Oak Ridge, Tennessee 37830, United States;* orcid.org/0000-0002-6875-0057

Nancy J. Dudney − *Chemical Sciences Division, Oak Ridge National Laboratory, Oak Ridge, Tennessee 37830, United States*

Tomonori Saito − *Chemical Sciences Division, Oak Ridge National Laboratory, Oak Ridge, Tennessee 37830, United States;* orcid.org/0000-0002-4536-7530

Complete contact information is available at: https://pubs.acs.org/10.1021/acsaem.0c02079

Notes

The authors declare no competing financial interest.

ACKNOWLEDGMENTS

This work was supported by the U.S. Department of Energy, Office of Science, Basic Energy Sciences, Materials Science and Engineering Division. J.N. and Y.Z. acknowledge support from Asst. Secretary, Energy Efficiency and Renewable Energy (EERE), Vehicle Technologies Office (VTO) under the Advanced Battery Materials Research (BMR) Program. The computational/simulation aspect of this work was performed at the Center for Nanophase Materials Sciences, a U.S. Department of Energy Office of Science User Facility. This research also used resources of the Oak Ridge Leadership Computing Facility, which is a DOE Office of Science User Facility supported under Contract DE-AC05-00OR22725.

REFERENCES

(1) Fan, L.; Wei, S.; Li, S.; Li, Q.; Lu, Y. Recent Progress of the Solid-State Electrolytes for High-Energy Metal-Based Batteries. *Adv. Energy Mater.* **2018**, *8*, No. 1702657.

(2) Sun, C.; Liu, J.; Gong, Y.; Wilkinson, D. P.; Zhang, J. Recent advances in all-solid-state rechargeable lithium batteries. *Nano Energy* **2017**, *33*, 363−386.

(3) Cheng, X. B.; Zhang, R.; Zhao, C. Z.; Zhang, Q. Toward Safe Lithium Metal Anode in Rechargeable Batteries: A Review. *Chem. Rev.* **2017**, *117*, 10403−10473.

(4) Xin, S.; You, Y.; Wang, S.; Gao, H.-C.; Yin, Y.-X.; Guo, Y.-G. Solid-State Lithium Metal Batteries Promoted by Nanotechnology: Progress and Prospects. *ACS Energy Lett.* **2017**, *2*, 1385−1394.

(5) Wang, S.; Xu, H.; Li, W.; Dolocan, A.; Manthiram, A. Interfacial Chemistry in Solid-State Batteries: Formation of Interphase and Its Consequences. *J. Am. Chem. Soc.* **2018**, *140*, 250−257.

(6) Pan, Q.; Barbash, D.; Smith, D. M.; Qi, H.; Gleeson, S. E.; Li, C. Y. Correlating Electrode-Electrolyte Interface and Battery Performance in Hybrid Solid Polymer Electrolyte-Based Lithium Metal Batteries. *Adv. Energy Mater.* **2017**, *7*, No. 1701231.

(7) Chinnam, P. R.; Fall, B.; Dikin, D. A.; Jalil, A.; Hamilton, C. R.; Wunder, S. L.; Zdilla, M. J. A Self-Binding, Melt-Castable, Crystalline Organic Electrolyte for Sodium Ion Conduction. *Angew. Chem., Int. Ed.* **2016**, *55*, 15254−15257.

(8) Cui, Y.; Liang, X.; Chai, J.; Cui, Z.; Wang, Q.; He, W.; Liu, X.; Liu, Z.; Cui, G.; Feng, J. High Performance Solid Polymer Electrolytes for Rechargeable Batteries: A Self-Catalyzed Strategy toward Facile Synthesis. *Adv. Sci.* **2017**, *4*, No. 1700174.

(9) Zeng, X. X.; Yin, Y. X.; Li, N. W.; Du, W. C.; Guo, Y. G.; Wan, L. J. Reshaping Lithium Plating/Stripping Behavior via Bifunctional Polymer Electrolyte for Room-Temperature Solid Li Metal Batteries. *J. Am. Chem. Soc.* **2016**, *138*, 15825−15828.

(10) Zhang, P.; Li, M.; Yang, B.; Fang, Y.; Jiang, X.; Veith, G. M.; Sun, X. G.; Dai, S. Polymerized Ionic Networks with High Charge Density: Quasi-Solid Electrolytes in Lithium-Metal Batteries. *Adv. Mater.* **2015**, *27*, 8088−8094.

(11) Zhang, H.; Li, C.; Piszcz, M.; Coya, E.; Rojo, T.; Rodriguez-Martinez, L. M.; Armand, M.; Zhou, Z. Single lithium-ion conducting solid polymer electrolytes: advances and perspectives. *Chem. Soc. Rev.* **2017**, *46*, 797−815.

(12) Lehmann, M. L.; Yang, G.; Nanda, J.; Saito, T. Well-designed Crosslinked Polymer Electrolyte Enables High Ionic Conductivity and Enhanced Salt Solvation. *J. Electrochem. Soc.* **2020**, *167*, No. 070539.

(13) Zhang, Z.; Sherlock, D.; West, R.; West, R.; et al. Cross-Linked Network Polymer Electrolytes Based on a Polysiloxane Backbone with Oligo(oxyethylene) Side Chains: Synthesis and Conductivity. *Macromolecules* **2003**, *36*, 9176−9180.

(14) Lu, Q.; He, Y. B.; Yu, Q.; Li, B.; Kaneti, Y. V.; Yao, Y.; Kang, F.; Yang, Q. H. Dendrite-Free, High-Rate, Long-Life Lithium Metal Batteries with a 3D Cross-Linked Network Polymer Electrolyte. *Adv. Mater.* **2017**, *29*, No. 1604460.

(15) Zhou, D.; He, Y.-B.; Liu, R.; Liu, M.; Du, H.; Li, B.; Cai, Q.; Yang, Q.-H.; Kang, F. In Situ Synthesis of a Hierarchical All-Solid-State Electrolyte Based on Nitrile Materials for High-Performance Lithium-Ion Batteries. *Adv. Energy Mater.* **2015**, *5*, No. 1500353.

(16) Li, X.; Qian, K.; He, Y.-B.; Liu, C.; An, D.; Li, Y.; Zhou, D.; Lin, Z.; Li, B.; Yang, Q.-H.; Kang, F. A dual-functional gel-polymer electrolyte for lithium ion batteries with superior rate and safety performances. *J. Mater. Chem. A* **2017**, *5*, 18888−18895.

(17) Chen, T.-L.; Sun, R.; Willis, C.; Morgan, B. F.; Beyer, F. L.; Elabd, Y. A. Lithium ion conducting polymerized ionic liquid pentablock terpolymers as solid-state electrolytes. *Polymer* **2019**, *161*, 128−138.

(18) Oh, B.; Vissers, D.; Zhang, Z.; West, R.; Tsukamoto, H.; Amine, K. New interpenetrating network type poly(siloxane-g-

ethylene oxide) polymer electrolyte for lithium battery. *J. Power Sources* **2003**, *119−121*, 442−447.
(19) Lin, D.; Yuen, P. Y.; Liu, Y.; Liu, W.; Liu, N.; Dauskardt, R. H.; Cui, Y. A Silica-Aerogel-Reinforced Composite Polymer Electrolyte with High Ionic Conductivity and High Modulus. *Adv. Mater.* **2018**, *30*, No. 1802661.
(20) Yu, J.; Wang, C.; Li, S.; Liu, N.; Zhu, J.; Lu, Z. Li(+) -Containing, Continuous Silica Nanofibers for High Li(+) Conductivity in Composite Polymer Electrolyte. *Small* **2019**, *15*, No. 1902729.
(21) Dirican, M.; Yan, C.; Zhu, P.; Zhang, X. Composite solid electrolytes for all-solid-state lithium batteries. *Mater. Sci. Eng., R* **2019**, *136*, 27−46.
(22) Liu, W.; Liu, N.; Sun, J.; Hsu, P. C.; Li, Y.; Lee, H. W.; Cui, Y. Ionic conductivity enhancement of polymer electrolytes with ceramic nanowire fillers. *Nano Lett.* **2015**, *15*, 2740−2745.
(23) Morris, M. A.; An, H.; Lutkenhaus, J. L.; Epps, T. H. Harnessing the Power of Plastics: Nanostructured Polymer Systems in Lithium-Ion Batteries. *ACS Energy Lett.* **2017**, *2*, 1919−1936.
(24) Lu, Y.; Tikekar, M.; Mohanty, R.; Hendrickson, K.; Ma, L.; Archer, L. A. Stable Cycling of Lithium Metal Batteries Using High Transference Number Electrolytes. *Adv. Energy Mater.* **2015**, *5*, No. 1402073.
(25) Bouchet, R.; Maria, S.; Meziane, R.; Aboulaich, A.; Lienafa, L.; Bonnet, J.-P.; Phan, T. N. T.; Bertin, D.; Gigmes, D.; Devaux, D.; Denoyel, R.; Armand, M. Single-ion BAB triblock copolymers as highly efficient electrolytes for lithium-metal batteries. *Nat. Mater.* **2013**, *12*, 452−457.
(26) Li, Z.; Lu, W.; Zhang, N.; Pan, Q.; Chen, Y.; Xu, G.; Zeng, D.; Zhang, Y.; Cai, W.; Yang, M.; Yang, Z.; Sun, Y.; Ke, H.; Cheng, H. Single ion conducting lithium sulfur polymer batteries with improved safety and stability. *J. Mater. Chem. A* **2018**, *6*, 14330−14338.
(27) Nguyen, H.-D.; Kim, G.-T.; Shi, J.; Paillard, E.; Judeinstein, P.; Lyonnard, S.; Bresser, D.; Iojoiu, C. Nanostructured multi-block copolymer single-ion conductors for safer high-performance lithium batteries. *Energy Environ. Sci.* **2018**, *11*, 3298−3309.
(28) Buss, H. G.; Chan, S. Y.; Lynd, N. A.; McCloskey, B. D. Nonaqueous Polyelectrolyte Solutions as Liquid Electrolytes with High Lithium Ion Transference Number and Conductivity. *ACS Energy Lett.* **2017**, *2*, 481−487.
(29) Cao, C.; Li, Y.; Feng, Y.; Long, P.; An, H.; Qin, C.; Han, J.; Li, S.; Feng, W. A sulfonimide-based alternating copolymer as a single-ion polymer electrolyte for high-performance lithium-ion batteries. *J. Mater. Chem. A* **2017**, *5*, 22519−22526.
(30) Bocharova, V.; Wojnarowska, Z.; Cao, P. F.; Fu, Y.; Kumar, R.; Li, B.; Novikov, V. N.; Zhao, S.; Kisliuk, A.; Saito, T.; Mays, J. W.; Sumpter, B. G.; Sokolov, A. P. Influence of Chain Rigidity and Dielectric Constant on the Glass Transition Temperature in Polymerized Ionic Liquids. *J. Phys. Chem. B* **2017**, *121*, 11511−11519.
(31) Shao, Z.; Jannasch, P. Single lithium-ion conducting poly-(tetrafluorostyrene sulfonate) − polyether block copolymer electrolytes. *Polym. Chem.* **2017**, *8*, 785−794.
(32) Cao, P.-F.; Wojnarowska, Z.; Hong, T.; Carroll, B.; Li, B.; Feng, H.; Parsons, L.; Wang, W.; Lokitz, B. S.; Cheng, S.; Bocharova, V.; Sokolov, A. P.; Saito, T. A star-shaped single lithium-ion conducting copolymer by grafting a POSS nanoparticle. *Polymer* **2017**, *124*, 117−127.
(33) Ahmed, F.; Choi, I.; Rahman, M. M.; Jang, H.; Ryu, T.; Yoon, S.; Jin, L.; Jin, Y.; Kim, W. Remarkable Conductivity of a Self-Healing Single-Ion Conducting Polymer Electrolyte, Poly(ethylene-co-acrylic lithium (fluoro sulfonyl)imide), for All-Solid-State Li-Ion Batteries. *ACS Appl. Mater. Interfaces* **2019**, *11*, 34930−34938.
(34) Diederichsen, K. M.; McShane, E. J.; McCloskey, B. D. Promising Routes to a High Li+ Transference Number Electrolyte for Lithium Ion Batteries. *ACS Energy Lett.* **2017**, *2*, 2563−2575.
(35) Zhou, D.; Tkacheva, A.; Tang, X.; Sun, B.; Shanmukaraj, D.; Li, P.; Zhang, F.; Armand, M.; Wang, G. Stable Conversion Chemistry-Based Lithium Metal Batteries Enabled by Hierarchical Multifunctional Polymer Electrolytes with Near-Single Ion Conduction. *Angew. Chem., Int. Ed.* **2019**, *58*, 6001−6006.
(36) Ren, C.; Liu, M.; Zhang, J.; Zhang, Q.; Zhan, X.; Chen, F. Solid-state single-ion conducting comb-like siloxane copolymer electrolyte with improved conductivity and electrochemical window for lithium batteries. *J. Appl. Polym. Sci.* **2018**, *135*, No. 45848.
(37) Monroe, C.; Newman, J. Dendrite Growth in Lithium/Polymer Systems. *J. Electrochem. Soc.* **2003**, *150*, A1377−A1384.
(38) Cao, C.; Li, Y.; Chen, S.; Peng, C.; Li, Z.; Tang, L.; Feng, Y.; Feng, W. Electrolyte-Solvent-Modified Alternating Copolymer as a Single-Ion Solid Polymer Electrolyte for High-Performance Lithium Metal Batteries. *ACS Appl. Mater. Interfaces* **2019**, *11*, 35683−35692.
(39) Luo, G.; Yuan, B.; Guan, T.; Cheng, F.; Zhang, W.; Chen, J. Synthesis of Single Lithium-Ion Conducting Polymer Electrolyte Membrane for Solid-State Lithium Metal Batteries. *ACS Appl. Energy Mater.* **2019**, *2*, 3028−3034.
(40) Deng, K.; Qin, J.; Wang, S.; Ren, S.; Han, D.; Xiao, M.; Meng, Y. Effective Suppression of Lithium Dendrite Growth Using a Flexible Single-Ion Conducting Polymer Electrolyte. *Small* **2018**, *14*, No. 1801420.
(41) Porcarelli, L.; Aboudzadeh, M. A.; Rubatat, L.; Nair, J. R.; Shaplov, A. S.; Gerbaldi, C.; Mecerreyes, D. Single-ion triblock copolymer electrolytes based on poly(ethylene oxide) and methacrylic sulfonamide blocks for lithium metal batteries. *J. Power Sources* **2017**, *364*, 191−199.
(42) Cai, W.; Zhang, Y.; Li, J.; Sun, Y.; Cheng, H. Single-ion polymer electrolyte membranes enable lithium-ion batteries with a broad operating temperature range. *ChemSusChem* **2014**, *7*, 1063−1067.
(43) Baum, P.; Meyer, W. H.; Wegner, G. Novel cation conductors based on rigid-rod poly(p-phenylene)s. *Polymer* **2000**, *41*, 965−973.
(44) Thelen, J. L.; Inceoglu, S.; Venkatesan, N. R.; Mackay, N. G.; Balsara, N. P. Relationship between Ion Dissociation, Melt Morphology, and Electrochemical Performance of Lithium and Magnesium Single-Ion Conducting Block Copolymers. *Macromolecules* **2016**, *49*, 9139−9147.
(45) Yu, Y.; Lu, F.; Sun, N.; Wu, A.; Pan, W.; Zheng, L. Single lithium-ion polymer electrolytes based on poly(ionic liquid)s for lithium-ion batteries. *Soft Matter* **2018**, *14*, 6313−6319.
(46) Feng, S.; Shi, D.; Liu, F.; Zheng, L.; Nie, J.; Feng, W.; Huang, X.; Armand, M.; Zhou, Z. Single lithium-ion conducting polymer electrolytes based on poly[(4-styrenesulfonyl)-(trifluoromethanesulfonyl)imide] anions. *Electrochim. Acta* **2013**, *93*, 254−263.
(47) Porcarelli, L.; Shaplov, A. S.; Salsamendi, M.; Nair, J. R.; Vygodskii, Y. S.; Mecerreyes, D.; Gerbaldi, C. Single-Ion Block Copoly(ionic liquid)s as Electrolytes for All-Solid State Lithium Batteries. *ACS Appl. Mater. Interfaces* **2016**, *8*, 10350−10359.
(48) Ma, Q.; Zhang, H.; Zhou, C.; Zheng, L.; Cheng, P.; Nie, J.; Feng, W.; Hu, Y. S.; Li, H.; Huang, X.; Chen, L.; Armand, M.; Zhou, Z. Single Lithium-Ion Conducting Polymer Electrolytes Based on a Super-Delocalized Polyanion. *Angew. Chem., Int. Ed.* **2016**, *55*, 2521−2525.
(49) Porcarelli, L.; Shaplov, A. S.; Bella, F.; Nair, J. R.; Mecerreyes, D.; Gerbaldi, C. Single-Ion Conducting Polymer Electrolytes for Lithium Metal Polymer Batteries that Operate at Ambient Temperature. *ACS Energy Lett.* **2016**, *1*, 678−682.
(50) Devaux, D.; Liénafa, L.; Beaudoin, E.; Maria, S.; Phan, T. N. T.; Gigmes, D.; Giroud, E.; Davidson, P.; Bouchet, R. Comparison of single-ion-conductor block-copolymer electrolytes with Polystyrene-TFSI and Polymethacrylate-TFSI structural blocks. *Electrochim. Acta* **2018**, *269*, 250−261.
(51) Li, S.; Mohamed, A. I.; Pande, V.; Wang, H.; Cuthbert, J.; Pan, X.; He, H.; Wang, Z.; Viswanathan, V.; Whitacre, J. F.; Matyjaszewski, K. Single-Ion Homopolymer Electrolytes with High Transference Number Prepared by Click Chemistry and Photoinduced Metal-Free Atom-Transfer Radical Polymerization. *ACS Energy Lett.* **2018**, *3*, 20−27.

https://dx.doi.org/10.1021/acsaem.0c02079
ACS Appl. Energy Mater. 2020, 3, 12540−12548

(52) Rohan, R.; Pareek, K.; Chen, Z.; Cai, W.; Zhang, Y.; Xu, G.; Gao, Z.; Cheng, H. A high performance polysiloxane-based single ion conducting polymeric electrolyte membrane for application in lithium ion batteries. *J. Mater. Chem. A* **2015**, *3*, 20267−20276.

(53) Snyder, J. F.; Hutchison, J. C.; Ratner, M. A.; Shriver, D. F. Synthesis of Comb Polysiloxane Polyelectrolytes Containing Oligoether and Perfluoroether Side Chains. *Chem. Mater.* **2003**, *15*, 4223−4230.

(54) Smith, A. L. Infrared spectra-structure correlations for organosilicon compounds. *Spectrochim. Acta* **1960**, *16*, 87−105.

(55) Legge, T. M.; Slark, A. T.; Perrier, S. Thermal stability of reversible addition-fragmentation chain transfer/macromolecular architecture design by interchange of xanthates chain-transfer agents. *J. Polym. Sci., Part A: Polym. Chem.* **2006**, *44*, 6980−6987.

(56) Postma, A.; Davis, T. P.; Li, G.; Moad, G.; O'Shea, M. S. RAFT Polymerization with Phthalimidomethyl Trithiocarbonates or Xanthates. On the Origin of Bimodal Molecular Weight Distributions in Living Radical Polymerization. *Macromolecules* **2006**, *39*, 5307−5318.

(57) Ratner, M. A.; Shriver, D. F. Ion transport in solvent-free polymers. *Chem. Rev.* **1988**, *88*, 109−124.

(58) Karan, N.; Pradhan, D.; Thomas, R.; Natesan, B.; Katiyar, R. Solid polymer electrolytes based on polyethylene oxide and lithium trifluoro- methane sulfonate (PEO−LiCF3SO3): Ionic conductivity and dielectric relaxation. *Solid State Ionics* **2008**, *179*, 689−696.

(59) Robitaille, C. D.; Fauteux, D. Phase Diagrams and Conductivity Characterization of Some PEO - LiX Electrolytes. *J. Electrochem. Soc.* **1986**, *133*, 315−325.

(60) Sun, X.-G.; Hou, J.; Kerr, J. B. Comb-shaped single ion conductors based on polyacrylate ethers and lithium alkyl sulfonate. *Electrochim. Acta* **2005**, *50*, 1139−1147.

(61) Li, H.; Han, C.; Huang, Y.; Huang, Y.; Zhu, M.; Pei, Z.; Xue, Q.; Wang, Z.; Liu, Z.; Tang, Z.; Wang, Y.; Kang, F.; Li, B.; Zhi, C. An extremely safe and wearable solid-state zinc ion battery based on a hierarchical structured polymer electrolyte. *Energy Environ. Sci.* **2018**, *11*, 941−951.

(62) Huang, S.; Wan, F.; Bi, S.; Zhu, J.; Niu, Z.; Chen, J. A Self-Healing Integrated All-in-One Zinc-Ion Battery. *Angew. Chem., Int. Ed.* **2019**, *58*, 4313−4317.

(63) Wu, K.; Huang, J.; Yi, J.; Liu, X.; Liu, Y.; Wang, Y.; Zhang, J.; Xia, Y. Recent Advances in Polymer Electrolytes for Zinc Ion Batteries: Mechanisms, Properties, and Perspectives. *Adv. Energy Mater.* **2020**, *10*, No. 1903977.

(64) Saha, P.; Datta, M. K.; Velikokhatnyi, O. I.; Manivannan, A.; Alman, D.; Kumta, P. N. Rechargeable magnesium battery: Current status and key challenges for the future. *Prog. Mater. Sci.* **2014**, *66*, 1−86.

(65) Sun, X. G.; Fang, Y.; Jiang, X.; Yoshii, K.; Tsuda, T.; Dai, S. Polymer gel electrolytes for application in aluminum deposition and rechargeable aluminum ion batteries. *Chem. Commun.* **2016**, *52*, 292−295.

(66) Bruce, P. G.; Hardgrave, M. T.; Vincent, C. A. The determination of transference numbers in solid polymer electrolytes using the Hittorf method. *Solid State Ionics* **1992**, *53−56*, 1087−1094.

(67) Cao, P.-F.; Li, B.; Yang, G.; Zhao, S.; Townsend, J.; Xing, K.; Qiang, Z.; Vogiatzis, K. D.; Sokolov, A. P.; Nanda, J.; Saito, T. Elastic Single-Ion Conducting Polymer Electrolytes: Toward a Versatile Approach for Intrinsically Stretchable Functional Polymers. *Macromolecules* **2020**, *53*, 3591−3601.

(68) Park, C. H.; Sun, Y.-K.; Kim, D.-W. Blended polymer electrolytes based on poly(lithium 4-styrene sulfonate) for the rechargeable lithium polymer batteries. *Electrochim. Acta* **2004**, *50*, 375−378.

(69) Van Humbeck, J. F.; Aubrey, M. L.; Alsbaiee, A.; Ameloot, R.; Coates, G. W.; Dichtel, W. R.; Long, J. R. Tetraarylborate polymer networks as single-ion conducting solid electrolytes. *Chem. Sci.* **2015**, *6*, 5499−5505.

(70) Zhang, J.; Wang, S.; Han, D.; Xiao, M.; Sun, L.; Meng, Y. Lithium (4-styrenesulfonyl) (trifluoromethanesulfonyl) imide based single-ion polymer electrolyte with superior battery performance. *Energy Storage Mater.* **2020**, *24*, 579−587.

(71) Meabe, L.; Goujon, N.; Li, C.; Armand, M.; Forsyth, M.; Mecerreyes, D. Single-Ion Conducting Poly(Ethylene Oxide Carbonate) as Solid Polymer Electrolyte for Lithium Batteries. *Batteries Supercaps* **2020**, *3*, 68−75.

(72) Yuan, H.; Luan, J.; Yang, Z.; Zhang, J.; Wu, Y.; Lu, Z.; Liu, H. Single Lithium-Ion Conducting Solid Polymer Electrolyte with Superior Electrochemical Stability and Interfacial Compatibility for Solid-State Lithium Metal Batteries. *ACS Appl. Mater. Interfaces* **2020**, *12*, 7249−7256.

(73) Borzutzki, K.; Thienenkamp, J.; Diehl, M.; Winter, M.; Brunklaus, G. Fluorinated polysulfonamide based single ion conducting room temperature applicable gel-type polymer electrolytes for lithium ion batteries. *J. Mater. Chem. A* **2019**, *7*, 188−201.

(74) Capiglia, C.; Saito, Y.; Kageyama, H.; Mustarelli, P.; Iwamoto, T.; Tabuchi, T.; Tukamot, H. 7Li and 19F diffusion coefficients and thermal properties of non-aqueous electrolyte solutions for rechargeable lithium batteries. *J. Power Sources* **1999**, *81−82*, 859−862.

(75) Valøen, L. O.; Reimers, J. N. Transport Properties of LiPF6-Based Li-Ion Battery Electrolytes. *J. Electrochem. Soc.* **2005**, *152*, A882−A891.

(76) Doyle, M.; Fuentes, Y. Computer simulations of a lithium-ion polymer battery and implications for higher capacity next-generation battery designs. *J. Electrochem. Soc.* **2003**, *150*, A706−A713.

(77) Zhao, J.; Wang, L.; He, X.; Wan, C.; Jiang, C. Determination of Lithium-Ion Transference Numbers. *J. Electrochem. Soc.* **2008**, *155*, A292−A296.

(78) Kido, R.; Ueno, K.; Iwata, K.; Kitazawa, Y.; Imaizumi, S.; Mandai, T.; Dokko, K.; Watanabe, M. Li+ Ion Transport in Polymer Electrolytes Based on a Glyme-Li Salt Solvate Ionic Liquid. *Electrochim. Acta* **2015**, *175*, 5−12.

(79) Hooper, R.; Lyons, L. J.; Mapes, M. K.; Schumacher, D.; Moline, D. A.; West, R. Highly Conductive Siloxane Polymers. *Macromolecules* **2001**, *34*, 931−936.

(80) He, Y.; Liu, N.; Kohl, P. A. High Conductivity, Lithium Ion Conducting Polymer Electrolyte Based on Hydrocarbon Backbone with Pendent Carbonate. *J. Electrochem. Soc.* **2020**, *167*, No. 100517.

(81) Ma, J. L.; Meng, F. L.; Yu, Y.; Liu, D. P.; Yan, J. M.; Zhang, Y.; Zhang, X. B.; Jiang, Q. Prevention of dendrite growth and volume expansion to give high-performance aprotic bimetallic Li-Na alloy-O_2 batteries. *Nat. Chem.* **2019**, *11*, 64−70.

https://dx.doi.org/10.1021/acsaem.0c02079
ACS Appl. Energy Mater. 2020, 3, 12540−12548